New Journal of Physics
The open-access journal for physics

Microscopic models of interacting Yang–Lee anyons

E Ardonne[1,5], J Gukelberger[2], A W W Ludwig[3], S Trebst[4] and M Troyer[2]

[1] Nordita, Roslagstullsbacken 23, 106-91 Stockholm, Sweden
[2] Theoretische Physik, ETH Zurich, 8093 Zurich, Switzerland
[3] Physics Department, University of California, Santa Barbara, CA 93106, USA
[4] Microsoft Research, Station Q, University of California, Santa Barbara, CA 93106, USA
E-mail: ardonne@kth.se

New Journal of Physics **13** (2011) 045006 (30pp)
Received 6 December 2010
Published 8 April 2011
Online at http://www.njp.org/
doi:10.1088/1367-2630/13/4/045006

Abstract. Collective states of interacting non-Abelian anyons have recently been studied mostly in the context of certain fractional quantum Hall states, such as the Moore–Read state proposed to describe the physics of the quantum Hall plateau at filling fraction $\nu = 5/2$. In this paper, we further expand this line of research and present non-unitary generalizations of interacting anyon models. In particular, we introduce the notion of Yang–Lee anyons, discuss their relation to the so-called 'Gaffnian' quantum Hall wave function and describe an elementary model for their interactions. A one-dimensional (1D) version of this model—a non-unitary generalization of the original golden chain model—can be fully understood in terms of an exact algebraic solution and numerical diagonalization. We discuss the gapless theories of these chain models for general $su(2)_k$ anyonic theories and their Galois conjugates. We further introduce and solve a 1D version of the Levin–Wen model for non-unitary Yang–Lee anyons.

[5] Author to whom any correspondence should be addressed.

Contents

1. Introduction

Over 30 years ago, Leinaas and Myrheim [1] pointed out that in systems confined to two spatial dimensions, particles with exotic exchange statistics, more general than those of bosons and fermions, are possible. Such particles with arbitrary exchange statistics were later named *anyons* by Wilczek [2]. Today it is widely believed that this possibility is indeed realized in the fractional quantum Hall effect. An even more intriguing form of statistics has recently received considerable attention, namely non-Abelian statistics, first proposed in a seminal paper by Moore and Read [3]. This form of statistics can occur in two-dimensional (2D) systems in which introducing excitations gives rise to a *macroscopic degeneracy* of states. Upon braiding the excitations, the wave functions (or better, the vector of wave functions) describing the system do not merely acquire an overall phase, but can actually transform into one another, as described by a unitary braid matrix acting within the degenerate manifold. In general, these braid matrices do not commute, hence the name non-Abelian statistics. While several systems have been theoretically proposed to exhibit quasiparticles with non-Abelian statistics, such as unconventional $p_x + \mathrm{i}p_y$ superconductors [4], rotating Bose–Einstein condensates (BEC) (see e.g. [5]), or certain heterostructures involving a novel class of materials, the so-called topological insulators [6], the system that is currently under intense experimental scrutiny is the fractional quantum Hall effect observed at filling fraction $\nu = 5/2$, with some evidence suggesting that this state is indeed non-Abelian in nature [7, 8].

An early attempt to describe this $\nu = 5/2$ quantum Hall state came in the form of the so-called Haldane–Rezayi wave function [9], which can be thought of as a d-wave paired BCS condensate of composite fermions—electrons with, in this case, two flux quanta attached. A peculiar feature of the Haldane–Rezayi state is that its gapless edge modes are described by a *non-unitary* conformal field theory (CFT) [10]–[14] with central charge $c = -2$. However,

non-unitary dynamics cannot describe a physical system as it would violate the basic principles of quantum mechanics. It has therefore been argued that in general the non-unitary nature of an edge state indicates that the underlying phase is not bulk gapped, but in fact critical [15]–[17] in which case the edge states lose their identity as they dissipate into the gapless bulk. For the Haldane–Rezayi state it indeed turns out that it does not describe a gapped topological phase, but rather the gapless state at a quantum phase transition between two gapped states—the Moore–Read quantum Hall state [3] and a so-called strong pairing quantum Hall phase [18]. Since the work of Haldane and Rezayi many other wave functions have been proposed, which appear to have non-unitary edge state theories [19]–[22]. One particularly well-known example is the so-called 'Gaffnian state' [17]. These proposed states typically arise from numerical studies of model Hamiltonians, for which it is often hard to determine whether they describe a gapped or gapless phase. The ultimate fate of these newly proposed states has therefore remained an active field of research.

In this paper, we will study the excitations of the putative quantum liquid described by such non-unitary wave functions from an 'anyon-model' perspective. Thus, we explore the physics that would occur if one were to assume that such excitations indeed exist and study in detail the collective behavior that would result. We refer to these excitations as non-unitary anyons and model the interaction between these anyons in the same way as was done in the unitary case [23]. It will turn out that the Hamiltonians one is led to consider for the non-unitary anyons are, not surprisingly, non-Hermitian. Nevertheless, the energy spectrum turns out to be completely real. One can hope that the results of such a study would shed some light on the questions surrounding the physical meaning of non-unitary anyons. Of course, in the context of 2D classical statistical mechanics, models having a non-unitary CFT describing a critical phase is a situation that often occurs—see, for instance, the (restricted) height models described in [24], which are generalizations of the 'restricted solid-on-solid' (RSOS) models [25]—and is not problematic.

Before closing this introduction with the outline of the paper, we should mention one additional point, which motivates the study of non-unitary anyon models: the concept of 'Galois conjugation' of CFTs. In short, the action of the Galois group relates different CFTs, which have the same number of fields, obeying the same fusion rules. The non-unitary models we encounter in this paper are in fact Galois conjugates of unitary CFTs, and thus the study of non-unitary anyons is closely related to the study of Galois conjugation in CFT [26, 27]. For the purposes of this paper, we will, however, not need to use any details of these connections.

This paper is organized as follows. In section 2, we discuss the Yang–Lee anyonic chains. We start by giving a review of the derivation of the Hamiltonian of the (ordinary, i.e. unitary) golden chain [23] of Fibonacci anyons in section 2.1, and a short mathematical description of the Galois-conjugated model, the so-called Yang–Lee chain in section 2.2, including an explicit derivation of their non-Hermitian, microscopic Hamiltonians, and discuss their relation to the 'golden chain' models of [23] via Galois conjugation. We continue in section 2.3 with a discussion of the algebraic structure underlying these microscopic Hamiltonians, which in turn allows for an analytical identification of their gapless theories in terms of certain non-unitary minimal models of CFT. We next present a number of exact, numerical results in section 2.4 and discuss the topological symmetry protecting the critical states in section 2.5 before rounding off with a discussion of the case of general level k in $\mathrm{su}(2)_k$ theories in section 2.6.

In section 3, we turn to 'doubled Yang–Lee' models and, in particular, a non-unitary generalization of the (unitary) high-genus ladder model that was previously studied for

Fibonacci anyons in [28], where we introduce the model in section 3.1. We then discuss the phase diagram in section 3.2, present the analytical solution at special critical points in section 3.3 and finish with exact numerical results in section 3.4.

The final section summarizes the results and discusses their relevance to hypothetical non-unitary topological phases. An appendix contains a detailed discussion of the conformal energy spectra at the four critical points discussed in the two models.

2. Yang–Lee chains

The focus of this paper is on anyonic models that are certain *non-unitary* generalizations of unitary non-Abelian anyon models, which have been extensively studied in the recent past [23], [28]–[35]. The basic constituents of the generalizations considered here are non-unitary, non-Abelian anyons. Like their unitary counterparts they carry a quantum number that corresponds to a generalized angular momentum in so-called $su(2)_k$ anyonic theories, which are certain deformations (see for instance [36]) of SU(2). We first concentrate on an elementary example where there is only a single anyon type by explicitly considering the anyon theory $su(2)_3$. In the unitary version of this theory the elementary degrees of freedom are often referred to as 'Fibonacci anyons', and it is their non-unitary counterparts that we term 'Yang–Lee anyons'. We will return to a discussion of the non-unitary generalizations for general $su(2)_k$ anyonic theories in section 2.6.

We start by quickly reviewing the basic construction of microscopic (chain) models of interacting non-Abelian anyons, following the ideas of the 'golden chain' model of [23] and the detailed exposition of [31]. The construction of these models proceeds in two steps. First, we describe the general structure of the Hilbert space of these models in a particular 'fusion chain' representation, which is identical for the unitary and non-unitary models. In a second step, we turn to the microscopic form of the Hamiltonian capturing interactions between the anyons. While this second step is quite similar for the unitary and non-unitary cases, the microscopic Hamiltonians for the two cases are distinct.

2.1. The golden chain

The elementary degrees of freedom in our microscopic model are the particle types (or generalized angular momenta) of the $su(2)_3$ anyonic theory. In its simplest form (considering only integer momenta), this theory contains a trivial particle (or vacuum state), which we denote by 1, and an anyonic particle, which we label as $\boldsymbol{\tau}$. These particles can form combined states according to the fusion rules

$$\mathbf{1} \times \mathbf{1} = \mathbf{1}, \quad \mathbf{1} \times \boldsymbol{\tau} = \boldsymbol{\tau}, \quad \boldsymbol{\tau} \times \boldsymbol{\tau} = \mathbf{1} + \boldsymbol{\tau}. \tag{1}$$

The non-Abelian nature of the anyonic $\boldsymbol{\tau}$-particle reveals itself in the *multiple* fusion outcomes when combining two of these particles.

Our chain model then consists of L such $\boldsymbol{\tau}$ particles in a 1D arrangement as depicted on the top of figure 1, where L denotes the number of sites of the chain. Since pairs of $\boldsymbol{\tau}$-particles can be fused into more than one state, such a system of L non-Abelian anyons spans a *macroscopic* manifold of states, i.e. a vector space whose dimension grows exponentially in the number of anyons. It is this manifold of states that constitutes the Hilbert space of our microscopic model.

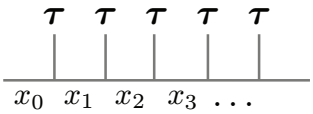

Figure 1. A chain of Fibonacci or Yang–Lee anyons (denoted by the τ's in the upper row). The set of admissible labelings $\{x_i\}$ along the fusion chain (lines) constitutes the Hilbert space of the Yang–Lee (and Fibonacci) chains.

Figure 2. The F-symbol describing the local change of basis.

To enumerate the states in the latter we define a so-called 'fusion chain' as illustrated at the bottom of figure 1. Here the original τ particles constituting the chain are denoted by the lines that are 'incoming' from above. The links in the fusion chain carry labels $\{x_i\}$ that again correspond to the particle types of the $su(2)_3$ theory. Reading the labels from left to right, a labeling is called admissible if at each vertex the fusion rules (1) of $su(2)_3$ are obeyed, i.e. a τ label is followed by either a $\mathbf{1}$ or τ label, while a $\mathbf{1}$ label is always followed by a τ label. Every such admissible labeling then constitutes one state in the Hilbert space of our anyonic chain. Considering periodic boundary conditions, i.e. $x_L = x_0$, it is straightforward to show that the dimension of the Hilbert space is given in terms of Fibonacci numbers as

$$\dim_L = \mathrm{Fib}_{L-1} + \mathrm{Fib}_{L+1},$$

where Fib_i denotes the ith Fibonacci number, defined by $\mathrm{Fib}_{i+1} = \mathrm{Fib}_i + \mathrm{Fib}_{i-1}$ and the initial conditions $\mathrm{Fib}_1 = \mathrm{Fib}_2 = 1$.

We now proceed to the second step of our construction, the derivation of a microscopic Hamiltonian. In doing so we follow the perspective of the original 'golden chain' model [23] in assuming that interactions between a pair of neighboring τ particles—mediated, for instance, by topological charge tunneling [37]—will result in an energy splitting of the two possible fusion outcomes in equation (1). Our Hamiltonian captures this splitting by projecting the fusion outcome of two neighboring τ particles onto the trivial fusion channel, i.e. assigning an energy of $E_{\mathbf{1}} = -1$ to the fusion of two τ particles into the trivial channel and an energy of $E_\tau = 0$ to the fusion into the τ channel. This anyonic Hamiltonian is thus reminiscent of the common Heisenberg Hamiltonian for SU(2) spins, which, for instance, projects two ordinary spin-1/2's onto the singlet channel and assigns a higher energy to the alternative triplet channel.

To explicitly derive the Hamiltonian in the Hilbert space of fusion chain labelings introduced above, we note that in this basis the fusion of two neighboring τ particles is not explicit. To get direct access to this fusion channel of two neighboring τ particles, we need to locally transform the basis as depicted in figure 2. The matrix describing this transformation is typically called the F-symbol, which can be thought of as an anyonic generalization of Wigner's $6j$-symbol for ordinary SU(2) spins. Its general form (in the absence of fusion multiplicities) is given in figure 3.

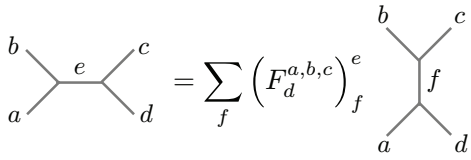

Figure 3. The general form of the F-symbol.

Assuming that we know the explicit form of the F-symbols (see the next section for more details), we can now explicitly derive the microscopic Hamiltonian in the fusion chain basis. After the basis transformation, the fusion channel of the two neighboring anyons is manifest, so by means of a simple projection we can assign an energy to each of the fusion channels. The final step left after this projection is to transform back to the original basis, which again employs the F-symbol.

To make the individual steps of this derivation more explicit, we consider the example of figure 2 in more detail. Let us specify the five possible labelings of three neighboring fusion chain labels x_{i-1}, x_i, x_{i+1}, where in figure 2 we depicted the case where the site label is $i = 2$,

$$|x_{i-1}, x_i, x_{i+1}\rangle \in \{|\mathbf{1}, \boldsymbol{\tau}, \mathbf{1}\rangle, \quad |\mathbf{1}, \boldsymbol{\tau}, \boldsymbol{\tau}\rangle, \quad |\boldsymbol{\tau}, \boldsymbol{\tau}, \mathbf{1}\rangle, \quad |\boldsymbol{\tau}, \mathbf{1}, \boldsymbol{\tau}\rangle, \quad |\boldsymbol{\tau}, \boldsymbol{\tau}, \boldsymbol{\tau}\rangle\}.$$

After performing the basis transformation shown in figure 2, the following labels satisfy the fusion rules at each vertex and thus form the new basis

$$|x_{i-1}, \tilde{x}_i, x_{i+1}\rangle \in \{|\mathbf{1}, \mathbf{1}, \mathbf{1}\rangle, \quad |\mathbf{1}, \boldsymbol{\tau}, \boldsymbol{\tau}\rangle, \quad |\boldsymbol{\tau}, \boldsymbol{\tau}, \mathbf{1}\rangle, \quad |\boldsymbol{\tau}, \mathbf{1}, \boldsymbol{\tau}\rangle, \quad |\boldsymbol{\tau}, \boldsymbol{\tau}, \boldsymbol{\tau}\rangle\},$$

where $\tilde{x}_i$ is the fusion channel of the two neighboring $\boldsymbol{\tau}$ particles. In the transformed basis, we can project onto the trivial channel, by means of a projection $P_{i,\mathbf{1}}$, where the subscript i denotes that we are acting on anyons i and $i+1$, while the label $\mathbf{1}$ denotes we are projecting onto the $\mathbf{1}$ channel. So, the part of the Hamiltonian acting on anyons i and $i+1$, which we denote by H^i, acts on the Hilbert space as

$$H^i\,|x_{i-1}, x_i, x_{i+1}\rangle = -\sum_{x_i'=\mathbf{1},\boldsymbol{\tau}} \left(F_{x_{i+1}}^{x_{i-1},\boldsymbol{\tau},\boldsymbol{\tau}}\right)_{\mathbf{1}}^{x_i} \left(F_{x_{i+1}}^{x_{i-1},\boldsymbol{\tau},\boldsymbol{\tau}}\right)_{x_i'}^{\mathbf{1}} |x_{i-1}, x_i', x_{i+1}\rangle. \tag{2}$$

Here, we have used that for the $\mathrm{su}(2)_k$ anyonic theories we are considering, the F-symbols are their own inverses. Moreover, we projected onto the $\mathbf{1}$ channel, which we favored, because of the overall minus sign. The total Hamiltonian then simply becomes the sum of (2) over all positions

$$H = \sum_{i=1}^{L} H^i, \tag{3}$$

where we assume periodic boundary conditions, i.e. $x_L = x_0$.

To describe the Hamiltonian of the various types of anyon chains we consider in this paper, we only have to specify the explicit form of the F-symbols (apart from the fusion rules, which determine the Hilbert space). The explicit form of the Hamiltonian then follows from equation (2).

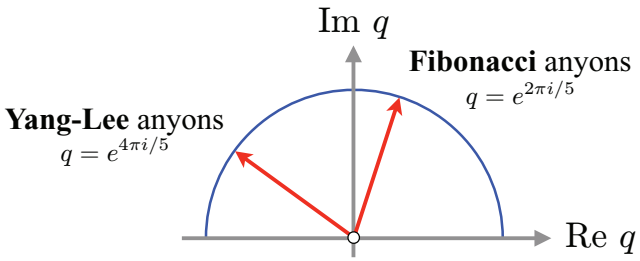

Figure 4. The q-deformation parameters of Fibonacci and Yang–Lee anyons correspond to different primitive roots of unity.

2.2. Galois conjugation and non-unitary models

Now that we have expressed the Hamiltonian in terms of the F-symbols, we should explain how to obtain the F-symbols for a given anyon theory. As stated, the F-symbols transform between two different fusion bases as illustrated in figure 3. As such, the exact form of these symbols can be determined self-consistently by identifying a circular sequence of basis transformations, which yield a set of strongly overconstrained nonlinear equations called the 'pentagon equations' (for a more detailed exposition see, for instance, [31, 38]). While finding a solution to these pentagon equations is in general a highly non-trivial task, it has been shown that they allow only for a *finite* set of inequivalent solutions, a property that goes under the name of 'Ocneanu rigidity', see for instance [39]. For the $\mathrm{su}(2)_k$ anyonic theories of interest here, the complete set of possible F-symbols can be found, e.g., in [40] where they were obtained by using quantum group techniques.

The different F-symbols are found to have a general form that depends on a single, so-called 'deformation parameter' q only. This deformation parameter has to be chosen appropriately [40] and it turns out that for the $\mathrm{su}(2)_k$ anyonic theory it must be one of the $(k+2)$th primitive roots of unity, i.e. of the form

$$q = \mathrm{e}^{p\cdot 2\pi \mathrm{i}/(k+2)}, \tag{4}$$

where the integer index p runs from $1 \leqslant p \leqslant (k+2)/2$ (and p and $k+2$ are relatively prime). The process of increasing the index p by one, i.e. going from one root of unity to the next, is what is usually referred to as Galois conjugation. For our example theory, $\mathrm{su}(2)_3$, we can thus identify two possible values for q, which are illustrated in figure 4. These two Galois-conjugated theories corresponding to deformation parameters, $q = \mathrm{e}^{2\pi \mathrm{i}/5}$ and $q = \mathrm{e}^{4\pi \mathrm{i}/5}$, then precisely correspond to the cases of Fibonacci and Yang–Lee anyons, respectively. The explicit form of the F-symbols and in particular the non-diagonal 2×2 matrix for $F_{\tau}^{\tau,\tau,\tau}$ can then be written [40] in terms of this deformation parameter q as

$$F_{\tau}^{\tau,\tau,\tau} = \begin{pmatrix} \dfrac{1}{q^{-1}+1+q} & \dfrac{1}{\sqrt{q^{-1}+1+q}} \\ \dfrac{1}{\sqrt{q^{-1}+1+q}} & \dfrac{q^{-1}-1+q}{q^{-1}+q} \end{pmatrix}. \tag{5}$$

For Fibonacci anyons we set $q = \mathrm{e}^{2\pi \mathrm{i}/5}$, in which case $q^{-1}+1+q = 1+2\cos(2\pi/5) = (1+\sqrt{5})/2 = \phi$ is the golden ratio, and the F-symbol becomes the *unitary* matrix

$$F_{\text{Fibonacci}} = \begin{pmatrix} \phi^{-1} & \phi^{-1/2} \\ \phi^{-1/2} & -\phi^{-1} \end{pmatrix}. \tag{6}$$

The golden ratio, of course, is one solution of the equation $x^2 = 1 + x$, which is an algebraic analogue of the fusion rule $\boldsymbol{\tau} \times \boldsymbol{\tau} = \mathbf{1} + \boldsymbol{\tau}$ of the $\mathrm{su}(2)_3$ anyonic theory. The process of taking the Galois conjugate of the original Fibonacci anyon model corresponds then simply to the substitution $\phi \to -1/\phi$, where $-1/\phi$ is the other solution to the equation $x^2 = 1 + x$. In terms of the deformation parameter q, this amounts to choosing the other possible value of $q = \mathrm{e}^{4\pi \mathrm{i}/5}$, which indeed yields $q^{-1} + 1 + q^1 = 1 + 2\cos(4\pi/5) = -1/\phi$. The F-symbol for Yang–Lee anyons thus becomes the (invertible) *non-unitary* matrix

$$F_{\text{Yang–Lee}} = \begin{pmatrix} -\phi & -\mathrm{i}\phi^{1/2} \\ -\mathrm{i}\phi^{1/2} & \phi \end{pmatrix}. \tag{7}$$

Having obtained the F-symbols in both the unitary and the non-unitary case, we can now write down the Hamiltonians for the Fibonacci and Yang–Lee chains. On the states $|x_{i-1}, x_i, x_{i+1}\rangle \in \{|\mathbf{1}, \boldsymbol{\tau}, \mathbf{1}\rangle, |\mathbf{1}, \boldsymbol{\tau}, \boldsymbol{\tau}\rangle, |\boldsymbol{\tau}, \boldsymbol{\tau}, \mathbf{1}\rangle\}$ both Hamiltonians act in the same diagonal way, $H^i = \mathrm{diag}\{-1, 0, 0\}$. Acting on the states $|x_{i-1}, x_i, x_{i+1}\rangle \in \{|\boldsymbol{\tau}, \mathbf{1}, \boldsymbol{\tau}\rangle, |\boldsymbol{\tau}, \boldsymbol{\tau}, \boldsymbol{\tau}\rangle\}$, the Hamiltonians take the following forms:[6]

$$\begin{aligned} H^i_{\text{Fibonacci}} &= -\begin{pmatrix} \phi^{-2} & \phi^{-3/2} \\ \phi^{-3/2} & \phi^{-1} \end{pmatrix}, \\ H^i_{\text{Yang–Lee}} &= -\begin{pmatrix} \phi^{2} & \mathrm{i}\phi^{3/2} \\ \mathrm{i}\phi^{3/2} & -\phi \end{pmatrix}. \end{aligned} \tag{8}$$

Before discussing these anyonic models in further detail, we note that while Galois conjugation changes some aspects of these models, i.e. the parameters in their respective Hamiltonians get 'Galois conjugated', this turns out to be a rather mild change, since the underlying algebraic structure of these models remains largely untouched. As a consequence, the non-unitary Yang–Lee chains allow for an analytic solution similar to their unitary counterparts as first obtained for the 'golden chain' model in [23]. We will discuss the details of this analytical solution and its resulting gapless theories in the next section.

2.3. Algebraic structure and analytical solution

In the original golden chain paper [23], it was shown that the Hamiltonian (3) based on the *unitary* F-symbols (6) can be exactly solved. Following a similar sequence of steps as in the unitary case, we show here that all non-unitary models allow for an exact analytical solution as well. We briefly outline these steps in the following; for a more detailed discussion, see [23, 31].

As a first step, it was noted that the operators H^i, i.e. the summands of the Hamiltonian, form (upon suitable normalization) a known representation [41] of the Temperley–Lieb algebra [42] with 'd-isotopy'-parameter d, namely $\mathbf{e}_i = -dH^i$, where $d = \phi$. These operators satisfy the Temperley–Lieb algebra

$$\mathbf{e}_i^2 = d\mathbf{e}_i, \quad \mathbf{e}_i\mathbf{e}_{i\pm1}\mathbf{e}_i = \mathbf{e}_i, \qquad [\mathbf{e}_i, \mathbf{e}_j] = 0 \quad \text{for } |i - j| \geqslant 2. \tag{9}$$

To show that this is the case, we will first map the Fibonacci and Yang–Lee chains onto so-called RSOS or 'height' models [25]. To do this, we first note that one can relate the Fibonacci

[6] We note that in a different gauge, the F-matrix (5) takes the form $F^{\boldsymbol{\tau},\boldsymbol{\tau},\boldsymbol{\tau}}_{\boldsymbol{\tau}} = \begin{pmatrix} \frac{1}{q} + q - 1 & \frac{1}{q} + q + 1 \\ 2(\frac{1}{q} + q) - 3 & -(\frac{1}{q} + q) + 1 \end{pmatrix}$. This F-matrix leads to different forms of the Fibonacci and Yang–Lee Hamiltonians as given in equation (8), but they nevertheless have identical energy spectra.

Table 1. Fusion rules of the $su(2)_3$ theory.

$\times$	0	1/2	1	3/2
0	0	1/2	1	3/2
1/2		0+1	1/2+3/2	1
1			0+1	1/2
3/2				0

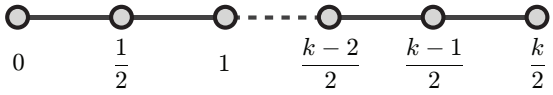

Figure 5. The allowed 'height' configurations of the chain models. This diagram is the Dynkin diagram of the Lie algebra $A_{k+1} = su(k+2)$. The Fibonacci and Yang–Lee anyons correspond to $k = 3$.

anyons to the anyonic theory $su(2)_3$, a theory with four particles (see section 2.6 for the more general case of $su(2)_k$), which can be labeled by their 'spin' $j = 0, 1/2, 1, 3/2$. The fusion rules of these particles are given in table 1. One immediately notes that the particle with $j = 1$ has the same fusion rules as the Fibonacci anyon. Indeed, the Fibonacci anyon model can be viewed as the 'integer subset' of the $su(2)_3$ theory. In addition, one notes that fusing a particle j with the particle $3/2$, one finds $j \times 3/2 = 3/2 - j$, swapping integer 'spin' to half-integer 'spin'. This allows one to map the Fibonacci chain, consisting of 'spin'-1 particles, to a chain of 'spin'-1/2 particles, by fusing the labels x_{2i-1} of the odd sites with the particle $3/2$. In this way, the new labels are constant labelings of a chain consisting of 'spin'-1/2 particles. Performing this map is advantageous, because the transformed Fibonacci chain can now directly be mapped onto a height model, in which the allowed heights take the values $0, 1/2, 1$ and $3/2$, which can be seen as the nodes of the Dynkin diagram A_4, which is given in figure 5.

The well-known Jones representation of the Temperley–Lieb algebra, acting on the Hilbert space of the (transformed) Fibonacci chain, can now be obtained by using the so-called modular S-matrix [41]. Explicitly, this representation is known to take on the following form:

$$\begin{aligned} \mathbf{e}_i \, |x_{i-1}, x_i, x_{i+1}\rangle &= \sum_{x_i'} \left((e_i)_{x_{i-1}}^{x_{i+1}}\right)_{x_i}^{x_i'} \left|x_{i-1}', x_i', x_{i+1}'\right\rangle, \\ \left((e_i)_{x_{i-1}}^{x_{i+1}}\right)_{x_i}^{x_i'} &= \delta_{x_{i-1},x_{i-1}'} \delta_{x_{i+1},x_{i+1}'} \frac{\sqrt{S_{0,x_i}}\sqrt{S_{0,x_i'}}}{\sqrt{S_{0,x_{i-1}}}\sqrt{S_{0,x_{i+1}}}}, \end{aligned} \tag{10}$$

where S_{j_1,j_2} is the modular S-matrix of the $su(2)_3$ theory, and the labels j_1, j_2 are the 'spins' of the corresponding particles, which in general take the values $0, 1/2, 1, \ldots, k/2$, and in terms of these, the S-matrix elements read

$$S_{j_1,j_2} = \sqrt{\frac{2}{k+2}} \sin\left(\frac{(2j_1+1)(2j_2+1)\pi}{k+2}\right). \tag{11}$$

In equation (10), the row label j_1 of the S-matrix elements which appears here takes on the value $j_1 = 0$, which is the correct value in the case of the (unitary) Fibonacci chain. In taking

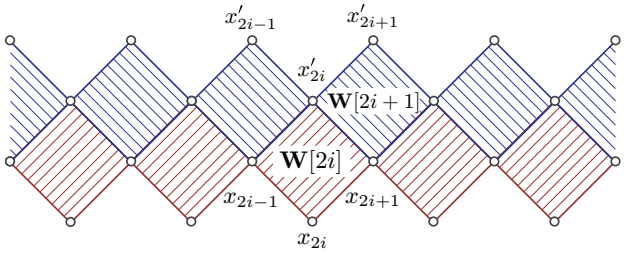

Figure 6. The two-row transfer matrix of the RSOS models.

the Galois conjugate, one has to replace this row label $j_1 = 0$ by the label $j_1 = 1$ (corresponding to a $\boldsymbol{\tau}$ particle (see also section 2.6)).

The action of the e_i's on the height states precisely corresponds to the action of the part of the Hamiltonian acting on the ket $|x_{i-1}, x_i, x_{i+1}\rangle$, which shows that the operators of the Hamiltonian of the Fibonacci chain indeed form a representation of the Temperley–Lieb algebra.

We will now employ this observation, and map the Fibonacci chain to an integrable, 2D statistical mechanics model, namely an RSOS model, which in the present case is based on the Dynkin diagram A_4—see figure 5. In an RSOS model, the degrees of freedom are the heights (or nodes of the Dynkin diagram). These heights live on the vertices of the lattice, with the constraint that heights of neighboring vertices correspond to nodes of the graph that are linked.

The two-row transfer matrix of the RSOS model (depicted in figure 6) can be written in terms of the plaquette weights of the square lattice, namely $\mathbf{T} = \mathbf{T}_2\mathbf{T}_1$, with

$$\mathbf{T}_1 = \prod_i \mathbf{W}[2i], \quad \mathbf{T}_2 = \prod_i \mathbf{W}[2i+1], \tag{12}$$

where the plaquette weights are of the form

$$\mathbf{W}[i]^{\vec{x}'}_{\vec{x}} = \left(\frac{\sin(\frac{p\pi}{k+2} - u)}{\sin(\frac{p\pi}{k+2})}\mathbf{1}^{\vec{x}'}_{\vec{x}} + \frac{\sin(u)}{\sin(\frac{p\pi}{k+2})}\mathbf{e}[i]^{\vec{x}'}_{\vec{x}}\right), \tag{13}$$

$$\mathbf{e}[i]^{\vec{x}'}_{\vec{x}} = \left(\prod_{j\neq i}\delta_{x'_j,x_j}\right)\left((e_i)^{x_{i+1}}_{x_{i-1}}\right)^{x'_i}_{x_i}, \tag{14}$$

with $\mathbf{1}^{\vec{x}'}_{\vec{x}} = \left(\prod_j \delta_{x'_j,x_j}\right)$ being the identity operator.

The new feature of the non-unitary models consists in the fact that equations (13) and (14) for the plaquette weight in the transfer matrix now involve a general integer $p = 2j_1 + 1$ labeling the primitive root of unity (4) beyond the unitary case of $p = 1$ (corresponding to $j_1 = 0$) studied earlier. For a general value of p, the Hamiltonian associated with this lattice model can be obtained by taking the extreme anisotropic limit, namely $u \to 0^+$ (see for instance [43]). One has

$$\mathbf{T} = \exp(-a(\mathbf{H} + c_1) + O(a^2)), \tag{15}$$

with $a = \frac{u}{d\sin(p\pi/(k+2))} \ll 1$ and c_1 an unimportant constant, which indeed gives that the Hamiltonian is of the form $H = -\frac{1}{d}\sum_i e_i$, establishing the mapping from the chain to the RSOS models.

We can now use the known results about the phases of the RSOS models, to find the behavior of the chain models. In the case of the Fibonacci anyons (i.e. when $k = 3$ and $p = 1$, which appear in the plaquette weights **W** and the parameter a), the antiferromagnetic golden chain Hamiltonian (Favouring the trivial fusion channel) can be obtained by taking the limit $u \to 0$ with u positive. The corresponding (exactly integrable) RSOS model [25] is critical and is known [25, 44] to be in the universality class of the tri-critical Ising model described by the minimal model $\mathcal{M}(4, 5)$ of CFT. For the ferromagnetic golden chain, which is obtained from the RSOS models with $0 < |u| \ll 1$ and u negative, the critical behavior then turns out [25, 44] to be in the universality class of the Z_3 parafermions corresponding to the minimal model variant[7] $\widetilde{\mathcal{M}}(5, 6)$.

In the case of the Galois-conjugated Yang–Lee anyonic chains (corresponding to $k = 3$ and $p = 2$), the same sequence of steps as above results in a mapping to another family of exactly integrable RSOS models [24] and in this case the gapless theories turn out be *non-unitary* minimal models [45, 46]. In this non-unitary case, the Hamiltonian can be obtained from the two-row transfer matrices, but in this case, both the antiferromagnetic and the ferromagnetic chains are obtained in the limit $u \to 0$ with positive u. The difference in the Hamiltonians stems from the sign-changes in the isotopy parameter d, namely from positive (but not necessarily bigger than one) in the antiferromagnetic case, to negative in the ferromagnetic case. The critical behavior in these two cases is then described by the (non-unitary) minimal models $\mathcal{M}(3, 5)$ and $\mathcal{M}(2, 5)$, respectively.

2.4. Numerical results

We have numerically studied the excitation spectra of the Yang–Lee chains by exact diagonalization of systems with up to $L = 32$ anyons, typically using periodic boundary conditions. These excitation spectra not only allow for an independent identification of the CFT describing the gapless collective state, as discussed in the previous section, but also reveal further details of the correspondence between continuous fields and microscopic observables. In particular, the low-energy states of a conformally invariant system can be identified with conformal fields and the excitation spectrum is expected to take the form

$$E = E_1 L + \frac{2\pi v}{L} \cdot \left(-\frac{c}{12} + h + \bar{h}\right), \tag{16}$$

where h and $\bar{h}$ are the (holomorphic and anti-holomorphic) conformal weights of a given CFT with central charge c. E_1 is a non-universal number, v a non-universal scale factor, and L the length of the chain. To match the excitation spectra of the Yang–Lee chains to these CFT predictions, we consider the family of so-called minimal models $M(p, p')$ (where p and p' are mutually prime) with central charge

$$c = 1 - \frac{6(p - p')^2}{pp'},$$

and conformal weights

$$h(r, s) = \frac{(rp - sp')^2 - (p - p')^2}{4pp'}, \tag{17}$$

[7] The minimal model variants $\widetilde{\mathcal{M}}(p, p')$ are discussed in more detail in section 3.2.

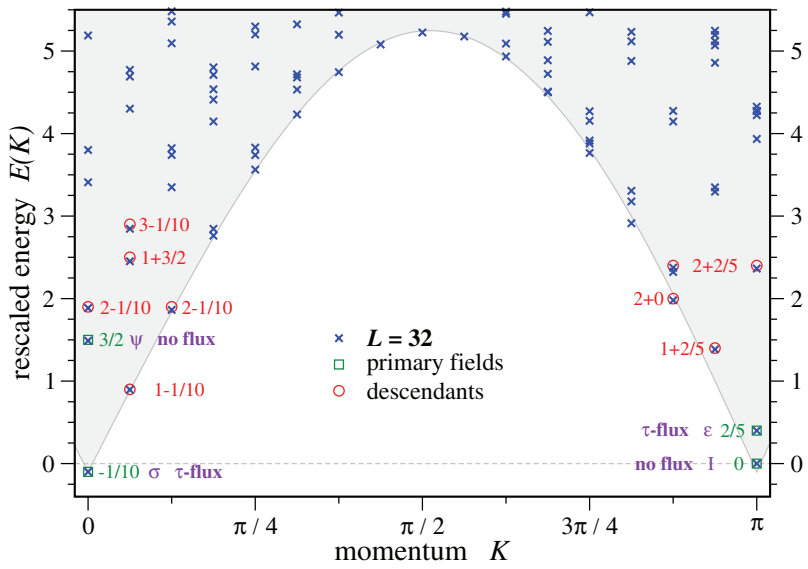

Figure 7. Conformal excitation spectrum of the 'antiferromagnetic' Yang–Lee chain. The spectrum matches the non-unitary minimal model $M(3,5)$ with central charge $c = -3/5$, which is often referred to as 'Gaffnian' theory. Primary fields $I, \sigma, \epsilon, \psi$ of this CFT are indicated by squares and descendant fields by circles. We also indicate the 'topological flux' of each energy eigenstate, which indicates the topological symmetry sector.

where the indices r and s are limited to $1 \leqslant r < p'$ and $1 \leqslant s < p$. We note that the labels (r, s) and $(p' - r, p - s)$ correspond to the same field.

In the following, we will discuss our numerically obtained excitation spectra for 'antiferromagnetic' and 'ferromagnetic' couplings, which are plotted in figures 7 and 8, respectively.

The antiferromagnetic chain. We first turn to the 'antiferromagnetic' chain, for which the pairwise anyon–anyon interaction energetically favors the trivial fusion channel

$$\boldsymbol{\tau} \times \boldsymbol{\tau} \to \mathbf{1}.$$

The CFT describing the critical behavior of this model is the non-unitary minimal model $\mathcal{M}(3,5)$ with central charge $c = -3/5$, which is also referred to as the 'Gaffnian' theory [17]. The four primary fields of this CFT and their respective scaling dimensions $\Delta = h + \bar{h}$ are

	σ	I	ϵ	ψ
Δ	$-1/10$	0	2/5	3/2

(18)

with the non-trivial fusion rules

$$\sigma \times \sigma = I + \epsilon \quad \sigma \times \epsilon = \sigma + \psi \quad \sigma \times \psi = \epsilon$$
$$\epsilon \times \epsilon = I + \epsilon \quad \epsilon \times \psi = \sigma$$
$$\psi \times \psi = I.$$

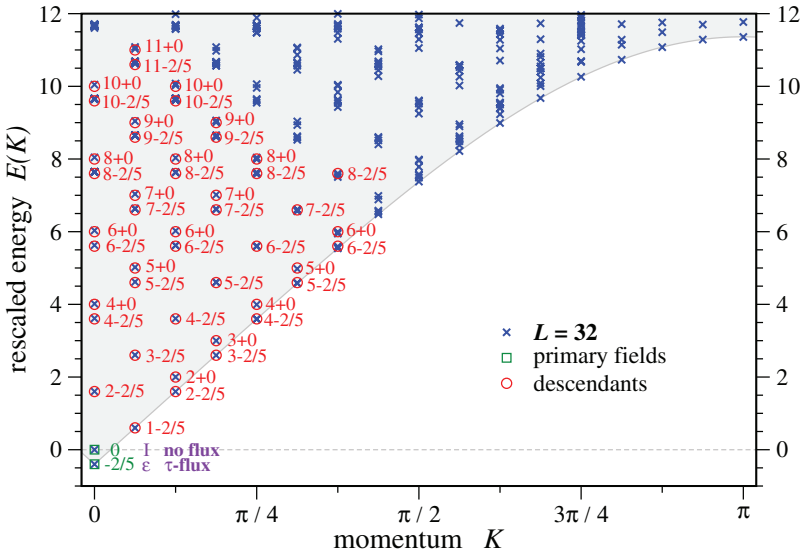

Figure 8. Conformal excitation spectrum of the 'ferromagnetic' Yang–Lee chain. The spectrum matches the non-unitary minimal model $M(2,5)$ with central charge $c = -22/5$, which is commonly referred to as 'Yang–Lee' theory. The primary fields I, ϵ of this CFT are indicated by squares and descendant fields by circles. We also indicate the 'topological flux' of each energy eigenstate, which indicates the topological symmetry sector.

Table 2. Kac table of conformal weights for the non-unitary minimal model $\mathcal{M}(3,5)$ and $\mathcal{M}(2,5)$. We only displayed fields with odd r labels, to avoid duplicates.

	$\mathcal{M}(3,5)$		$\mathcal{M}(2,5)$
$h(r,s)$	$s=1$	2	$s=1$
$r=1$	0	3/4	0
3	1/5	$-1/20$	$-1/5$

For completeness, we give the conformal dimensions of the fields (with minimal model labeling) in table 2, and note that this model is a particular Galois conjugate of the $su(2)_3$ CFT.

To identify the gapless theory numerically, we typically perform the following procedure: we first look at the two lowest energy eigenvalues in the spectrum, E_0 and E_1, and by identifying the energy gap $\Delta E = E_1 - E_0$ with the difference of the two lowest scaling dimensions, we can identify the non-universal scale factor $2\pi v/L$ in (16), which we subsequently set to 1, thereby rescaling the entire energy spectrum. This identification of the two lowest-energy eigenvalues with conformal operators also allows us to identify an overall energy shift, e.g. setting the energy of the trivial operator I with scaling dimension $h(1,1)+\bar{h}(1,1) = 0$ to zero. In the case at hand, there is only one negative scaling dimension, so the lowest energy corresponds to $-2h_{\min} = -1/10$, while the second lowest state corresponds to the identity operator, with zero energy. At this point, all the energies are fixed, and indeed the rescaled and shifted numerical

spectrum is found to reproduce the position of the (other) primary fields (indicated by green squares in figure 7), as well as a number of descendants (indicated by red circles in figure 7).

The ferromagnetic chain. We now turn to the 'ferromagnetic' chain, for which the pairwise anyon–anyon interaction energetically favors the $\boldsymbol{\tau}$-fusion channel

$$\boldsymbol{\tau} \times \boldsymbol{\tau} \to \boldsymbol{\tau}.$$

The critical theory is the non-unitary minimal model $\mathcal{M}(2, 5)$ with central charge $c = -22/5$, which is commonly referred to as the 'Yang–Lee' theory [47, 48]. The two primary fields of this CFT and their respective scaling dimensions $\Delta = h + \bar{h}$ are

	I	ϵ
Δ	0	$-2/5$

(19)

with the non-trivial fusion rule

$$\epsilon \times \epsilon = I + \epsilon.$$

Again we give the conformal dimensions of the fields (with minimal model labeling) in table 2 for completeness.

The spectrum of this theory, after the appropriate shift and rescaling of the energy, is displayed in figure 8, which beautifully reproduces the primary fields as well as descendants to a high level, constituting the spectrum of the Yang–Lee model.

2.5. *Topological symmetry*

Before considering further generalizations of the Yang–Lee chains, we wish to mention another peculiarity of these anyonic chains. Like their unitary counterparts the Yang–Lee chains exhibit an unusual, non-local symmetry. This symmetry, which was dubbed a 'topological symmetry' in the context of the golden chain model [23], corresponds to the operation of commuting a $\boldsymbol{\tau}$ particle through all particles of the chain. The so-defined operator, which we denote by Y, is found to commute with the Hamiltonian and for the $\mathrm{su}(2)_3$ theory has two distinct eigenvalues, thus defining two symmetry sectors. Its matrix form is given by

$$\langle x'_0, \ldots, x'_{L-1}|Y|x_0, \ldots, x_{L-1}\rangle = \prod_{i=0}^{L-1} \left(F^{\boldsymbol{\tau} x_i \boldsymbol{\tau}}_{x'_{i+1}}\right)^{x'_i}_{x_{i+1}}. \tag{20}$$

This definition solely in terms of the F-symbols immediately suggests a generalization of this symmetry to the case of the non-unitary Yang–Lee models studied above by simply replacing the F-symbols with their non-unitary counterparts (7). For both the unitary and non-unitary variants the two eigenvalues of the respective topological symmetry operator are $y_1 = \phi$ and $y_2 = -1/\phi$. In the unitary case these are identified as no-flux or $\boldsymbol{\tau}$-flux symmetry sectors, respectively. This assignment is simply reversed in the Galois-conjugated, non-unitary case.

For the unitary models it has been demonstrated that this topological symmetry *protects* the gapless ground state of the interacting anyon chain model [34]: it was shown that all relevant operators (in a renormalization group sense) that have otherwise identical quantum numbers as the ground state, e.g. the same momentum, fall into different topological symmetry sectors. We have performed a similar symmetry analysis for the Yang–Lee chains at hand. For chains with either antiferromagnetic or ferromagnetic couplings, we have evaluated the eigenvalue of the topological symmetry Y for all eigenvectors of the Hamiltonian and thereby assigned

topological symmetry sectors to the primary fields of the CFT describing their energy spectrum. These assignments are given in figures 7 and 8 for antiferromagnetic and ferromagnetic chain couplings, respectively. A situation similar to the unitary models emerges: for both signs of the coupling the ground state with conformal dimension $h+\bar{h}<0$ is found to be in the topologically non-trivial (or $\boldsymbol{\tau}$-flux) sector, while all other primary fields with the same momentum are found to be in the topologically trivial (or no-flux) sector.

For the unitary anyon chains, this topological protection mechanism has subsequently been cast in a broader physical picture [34] interpreting the gapless modes of the anyonic chains as edge states at the spatial interface of two topological liquids, and the conclusion that anyon–anyon interactions result in a splitting of the topological degeneracy for a set of non-Abelian anyons and the nucleation of a distinct topological liquid within the parent liquid of which the anyons are quasiparticle excitations [34, 35]. The similarity of our results for the topological symmetry properties of the non-unitary anyon chains thus raises the question as to whether a similar interpretation would also hold for the non-unitary systems at hand.

2.6. $\mathrm{su}(2)_k$ *theories and generalized Galois conjugation*

While we have focused our discussion in the preceding sections on the Fibonacci/Yang–Lee anyonic theories for which $k=3$, our results can be readily generalized to a much larger class of anyonic theories, the so-called $\mathrm{su}(2)_k$ Chern–Simons theories. These theories, which are certain quantum deformations [36] of SU(2), have a *finite* number of representations that are identified with the (anyonic) particle content of the theory. For a given (integer) deformation parameter k these representations/particles are labeled by a generalized angular momentum

$$j=0,\frac{1}{2},1,\ldots,\frac{k-1}{2},\frac{k}{2}.$$

The fusion rules for combining two of these momenta (or their associated particles) then resemble the tensor product rules of ordinary SU(2) angular momenta and explicitly read

$$j_1\times j_2=\sum_{j_3=|j_1-j_2|}^{\min(j_1+j_2,k-j_1-j_2)} j_3. \tag{21}$$

For all $k\leqslant 2$ the first non-trivial fusion rule (i.e. a fusion rule with multiple fusion outcomes) is encountered for the particle carrying generalized angular momentum $j=1/2$, for which one finds

$$\tfrac{1}{2}\times\tfrac{1}{2}=0+1. \tag{22}$$

Upon further inspection of the fusion rules (see table 1 for an example), one notes that for anyonic theories with odd k one can map all half-integer representations onto integer representations by fusing the half-integer representations with the highest representation of the theory, the so-called 'simple current' with angular momentum $\frac{k}{2}$. In particular, this mapping identifies the fusion rules of the particle carrying angular momentum $j=1/2$ with those of the particle carrying angular momentum $j=(k-1)/2$ and equation (22) becomes

$$\frac{k-1}{2}\times\frac{k-1}{2}=0+1. \tag{23}$$

Note that for odd k the fusion rules are now given entirely in terms of integer representations[8]. For the $su(2)_{k=3}$ theory this mapping thus turns the fusion rules of the $j = 1/2$ particle into those of the $j = 1$ particle, i.e. $1 \times 1 = 0 + 1$, which is the momentum representation of the non-trivial fusion rule in equation (1). One can thus equally identify the $\boldsymbol{\tau}$ particle of the Fibonacci/Yang–Lee theories with both the $j = 1$ and $j = 1/2$ angular momenta in $su(2)_3$.

The $su(2)_k$ generalizations of the Fibonacci/Yang–Lee chains, which we want to consider in the following, are chains of particles carrying angular momentum $j = 1/2$, which we can alternatively identify with particles carrying angular momentum $j = (k-1)/2$. The microscopic chain model is then constructed in an identical way to what we outlined for the case of the Fibonacci/Yang–Lee theories in section 2, i.e. we first build a Hilbert space by considering admissible labelings of the fusion chain basis for an incoming $j = 1/2$ (or $j = (k-1)/2$) particle and then derive a Hamiltonian via the local projection onto one of the two fusion outcomes in equation (22) or (23), respectively. Our notion for the sign of the interaction also remains unchanged, with 'antiferromagnetic' interactions favoring fusion of neighboring particles into a total $j = 0$ state and 'ferromagnetic' interactions favoring fusion into a total $j = 1$ state.

Unitary models. For the unitary case, such $su(2)_k$ generalizations of the golden chain model were first discussed in [23] and further explored in [34]. Like their $su(2)_3$ counterpart these generalized anyon chains are found to be exactly solvable and their gapless collective states can be described in terms of CFTs. To be specific, the critical theory for the generalized antiferromagnetic chains is known to be the minimal model $\mathcal{M}(k+1, k+2)$ with central charge $c = 1 - 6/((k+1)(k+2))$, while for ferromagnetic chains it is known to be the Z_k parafermion theory with central charge $c = 2(k-1)/(k+2)$. In both cases, the terms in the Hamiltonian are found to form a Temperley–Lieb algebra with isotopy parameter $d = 2\cos(\pi/(k+2))$.

Non-unitary models. In turning to the Galois-conjugated models of these unitary $su(2)_k$ anyon chains, we first recall that for a given $su(2)_k$ anyonic theory there are several allowed q deformation parameters (see also section 2.2)

$$q = \mathrm{e}^{p \cdot 2\pi \mathrm{i}/(k+2)}, \tag{24}$$

as illustrated in figure 9. For each integer index $1 \leqslant p \leqslant (k+2)/2$ (and the further restriction that p and $k+2$ are relatively prime) the corresponding q deformation parameter establishes a solution of the pentagon equations of the underlying $su(2)_k$ theory and defines the explicit form of the F-symbols. All the unitary $su(2)_k$ models discussed above correspond to the first primitive root, i.e. $p = 1$, in this sequence. The other primitive roots (with $p \geqslant 2$) then give rise to the Galois-conjugated models with non-unitary F-symbols and non-Hermitian microscopic Hamiltonians constructed using these F-symbols. In particular, we note that for $k = 2$ there is no such Galois-conjugated theory, for $k = 3$ there is exactly one Galois-conjugated theory (the Yang–Lee theory discussed above) and for $k \geqslant 4$ there are in general *multiple* Galois-conjugated theories.

Like their unitary counterparts all Galois-conjugated $su(2)_k$ chain models permit an analytical solution. Since the line of argument closely follows the one given in section 2.3 for $k = 3$, we will be brief here, and merely state the main arguments and results. To simplify the presentation we will further focus our arguments to anyonic theories with odd k, which

[8] More generally, one finds that the integer representations form a closed subset under the fusion rules of equation (21).

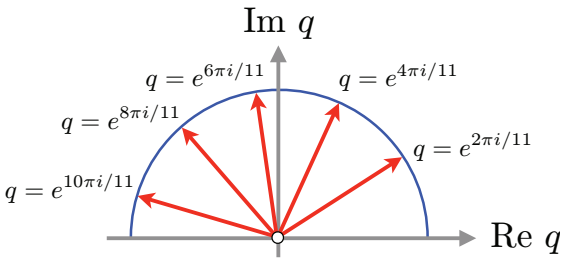

Figure 9. The q-deformation parameters for a general su(2)$_k$ theory correspond to different primitive roots of unity. Only the first primitive root in this sequence, e.g. $q = \mathrm{e}^{2\pi \mathrm{i}/11}$ in the illustrated example of $k = 9$, gives rise to a unitary model.

allows us to restrict the discussion to those which possess only integer (not half-integer) values of 'angular momenta' j. (Even values of k work in an analogous manner.) The Galois-conjugated su(2)$_k$ chain models can then be directly mapped onto the height representations of certain RSOS models where the heights take the values $0, 1/2, \ldots, k/2$ in the Dynkin diagram A_k illustrated in figure 5. The Hamiltonian terms acting in this height representation then again form a Temperley–Lieb algebra [41] with an isotopy parameter that now turns out to depend on the sign of the interactions. For antiferromagnetic coupling this generalized isotopy parameter is found to be $d = 2\cos(p\pi/(k+2))$ and the conformal theory describing the gapless interacting system is the non-unitary minimal model $\mathcal{M}(k+2-p, k+2)$ with central charge[9] $c = 1 - \frac{6p^2}{(k+2)(k+2-p)}$. For ferromagnetic couplings the isotopy parameter becomes $d = 2\cos\left(\frac{(k+2-p)\pi}{k+2}\right)$ and the gapless theory is the non-unitary minimal model $\mathcal{M}(p, k+2)$ with central charge $c = 1 - \frac{6(k+2-p)^2}{p(k+2)}$. In the case of the Galois-conjugated models, the central charges are related to the quantum dimensions in the following way [41, 49, 50]. Writing the quantum dimension as $d = 2\cos(p\pi/(k+2)) = 2\cos(\pi/\delta)$ (where δ is a fraction for the Galois-conjugated models), one can obtain the central charge via $c = 1 - \frac{6}{\delta(\delta-1)}$. Note that this is also the correct result for the antiferromagnetic unitary chain with $p = 1$, but the central charge for the ferromagnetic unitary chains is given by $c = 2 - 6/\delta$.

Our results for unitary and non-unitary models are summarized in table 3. We note that for $p = 2$ and $k = 3$, we exactly reproduce the results for the Yang–Lee chains discussed above.

3. Doubled Yang–Lee models

3.1. The ladder Hamiltonian

In this section, we turn to 'quantum double' variants of the anyonic chains discussed in section 2. The unitary incarnations of these quantum double models have been introduced in the context of exotic quantum phase transitions in time-reversal invariant systems that are driven by topology fluctuations [28]. The specific model is defined on a ladder geometry, shown in figure 10.

[9] The identification of the critical theories between regions III and IV in the Forrester–Baxter RSOS model [24] with these non-unitary minimal models was obtained in [45, 46].

Table 3. Overview of the gapless theories for the various chain models.

Coupling	CFT	Central charge	d-isotopy
$su(2)_k$ chains			
AFM	$\mathcal{M}(k+1,k+2)$	$c=1-\frac{6}{(k+1)(k+2)}$	$2\cos\left(\frac{\pi}{k+2}\right)$
FM	$\mathcal{Z}_k$ parafermion	$c=2\frac{k-1}{k+2}$	$2\cos\left(\frac{\pi}{k+2}\right)$
Yang–Lee chains			
AFM	$\mathcal{M}(k,k+2)$	$c=1-\frac{24}{k(k+2)}$	$2\cos\left(\frac{2\pi}{k+2}\right)$
FM	$\mathcal{M}(2,k+2)$	$c=1-\frac{3k^2}{k+2}$	$2\cos\left(\frac{k\pi}{k+2}\right)$
Generalized Galois conjugates with $2\leqslant p<(k+2)/2$			
AFM	$\mathcal{M}(k+2-p,k+2)$	$c=1-\frac{6p^2}{(k+2-p)(k+2)}$	$2\cos\left(\frac{p\pi}{k+2}\right)$
FM	$\mathcal{M}(p,k+2)$	$c=1-\frac{6(k+2-p)^2}{p(k+2)}$	$2\cos\left(\frac{(k+2-p)\pi}{k+2}\right)$

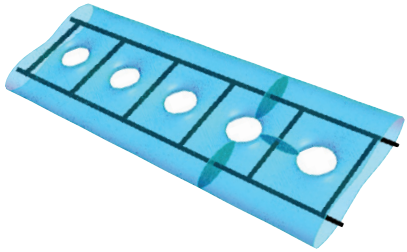

Figure 10. The geometry of the Fibonacci and Yang–Lee ladders. To discuss the physics, it is enlightening to 'thicken' the ladder and consider the 2D surface thus obtained.

The Hamiltonian

$$H_{\text{ladder}}=-J_r\sum_{\text{rungs } r}\delta_{l(r),\mathbf{1}}-J_p\sum_{\text{plaquettes } p}\delta_{\phi(p),\mathbf{1}} \tag{25}$$

consists of two competing terms.

The first term favors the trivial label $\mathbf{1}$ on each rung of the ladder, while the second term favors the no-flux state for all plaquettes. As shown in [28], the projector onto the flux through a square plaquette can be expressed in terms of the unitary/non-unitary F-matrices in equations (6) and (7). This term is equivalent to the plaquette term in the Levin–Wen models [51], which are defined on a different lattice, the honeycomb lattice.

Explicitly, the plaquette term reads

$$\delta_{\phi(p),\mathbf{1}}\left|\begin{array}{ccc} a & \alpha & b \\ & \delta & \beta \\ d & \gamma & c \end{array}\right\rangle=\sum_{s=\mathbf{1},\boldsymbol{\tau}}\frac{d_s}{D^2}\sum_{\alpha',\beta',\gamma',\delta'}\left(F_a^{\alpha' s\delta}\right)_\alpha^{\delta'}\left(F_b^{\beta' s\alpha}\right)_\beta^{\alpha'}\left(F_c^{\gamma' s\beta}\right)_\gamma^{\beta'}\left(F_d^{\delta' s\gamma}\right)_\delta^{\gamma'}\left|\begin{array}{ccc} a & \alpha' & b \\ & \delta' & \beta' \\ d & \gamma' & c \end{array}\right\rangle, \tag{26}$$

where d_s denotes the quantum dimension of particle type s, i.e. $d_{\mathbf{1}}=1$ and $d_{\boldsymbol{\tau}}=\phi$. D denotes the total quantum dimension, $D=\sqrt{d_{\mathbf{1}}^2+d_{\boldsymbol{\tau}}^2}=\sqrt{2+\phi}$ for Fibonacci (as well as Yang–Lee)

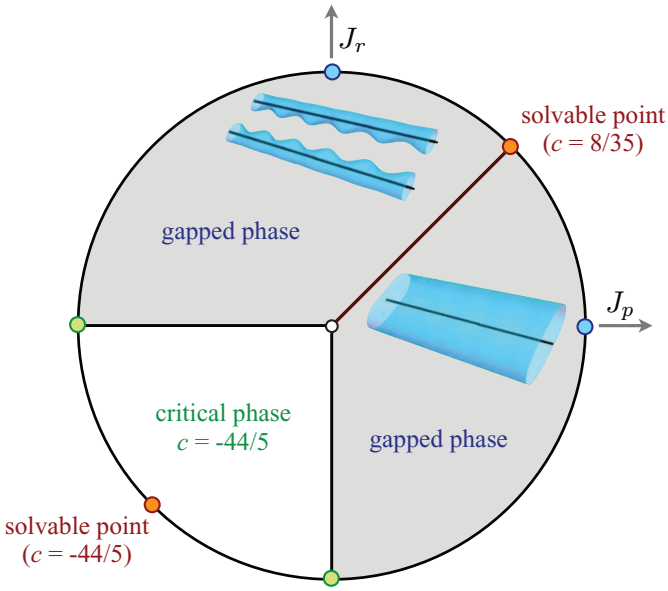

Figure 11. Phase diagram of the doubled Yang–Lee chain.

anyons. The Latin and Greek labels denote the degrees of freedom, and any of these takes one of the values $\{\mathbf{1}, \boldsymbol{\tau}\}$. We note that the Hilbert space of the ladder models consists of all possible labelings of the rungs and the legs, such that at each vertex, the Fibonacci fusion rules are obeyed.

With this description of the ladder models, we can easily go back and forth between the Fibonacci anyon ladder and the Yang–Lee anyon ladder, simply by choosing the corresponding set of F-symbols, namely equation (6) or (7), respectively.

3.2. The phase diagram

To discuss the phase diagram of both the unitary and the Galois-conjugated model, shown in figure 11, we parameterize the couplings $J_r = \sin\theta$ and $J_p = \cos\theta$ in terms of an angle θ.

We start with the first gapped phase, for $\pi/4 < \theta < \pi$, most easily discussed at the special point $\theta = \pi/2$, or $J_r = 1$ and $J_p = 0$. In the ground state at this point, all rungs have the trivial label. In the 2D surface geometry, this means that no $\boldsymbol{\tau}$-fluxes go through the rungs, implying that the rungs can be completely pinched off, changing the geometry to that of two, disconnected cylinders, one for each leg of the ladder. Each of the cylinders accommodates two ground states, either with or without $\boldsymbol{\tau}$-flux, leading to a fourfold ground state degeneracy. The lowest (gapped) excited state consists of configurations where one rung of the ladder 'contains' a $\boldsymbol{\tau}$-flux.

In the other extended gapped phase, for $-\pi/2 < \theta < \pi/4$, let us discuss the special point $\theta = 0$, or $J_p = 1$ and $J_r = 0$. Here the situation is reversed, and no $\boldsymbol{\tau}$-fluxes go through the *plaquettes*. Thus, they can be closed off, giving rise to a geometry consisting of a single cylinder. Again, this cylinder can accommodate two ground states, with or without flux, resulting in a twofold degenerate ground state. The lowest (gapped) excited state consists of configurations with a single $\boldsymbol{\tau}$-flux going through a plaquette, effectively piercing a hole through the cylinder.

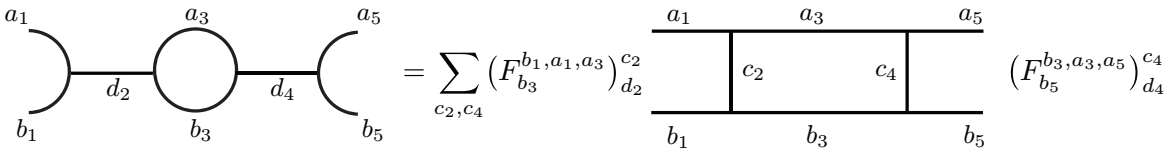

Figure 12. Basis transformation of the ladder model.

Precisely at the point where both couplings are equal in strength, the gap closes and the system is critical. At this point, the geometry is fluctuating at all length scales, interpolating between the two extremes of having one or two cylinders, respectively. In addition, also precisely at this point, the (critical) model is exactly solvable, as explained in the next section.

Finally, for $\pi < \theta < 3\pi/2$, there is an extended critical region, which is characterized by another exactly solvable point, at $\theta = 5\pi/4$, where both couplings are again of equal strength, but negative.

3.3. Analytical solution

The analytic solution of the Fibonacci ladder model at the two exactly solvable points has been described in detail in (the supplementary material of) [28]. Thus, we will be rather brief here, and point out some of the crucial steps of the mapping of the ladder model onto an exactly solved (RSOS) model. We will then quickly mention in which way this solution for the unitary Fibonacci case is changed, if one takes the Galois conjugate, to go to the case of the Yang–Lee ladder model. The most important step in the analytic solution of the model is to perform a basis transformation on the Hilbert space. After this transformation, the model can be mapped onto an RSOS model, where in this case, the allowed height variables lie on the vertices of the Dynkin diagram of the Lie algebra D_6, as it will turn out. This model is exactly solvable, both in the original, as well as the Galois-conjugated case.

The basis transformation proceeds as follows. At each rung, one applies an F-transformation, changing the basis building blocks of the ladder as illustrated in figure 12. Thus, we can express the Hilbert space in terms of the variables $\{a_{2i-1}, b_{2i-1}, c_{2i}\}$ or, equivalently, in terms of the variables $\{a_{2i-1}, b_{2i-1}, d_{2i}\}$, as displayed in figure 12. The mapping to the RSOS model is performed in terms of the latter variables. In particular, one can determine which 'values' the links can take on the even and odd sublattices. The variables on the even sublattice d_{2i} can take the values $\{\mathbf{1}, \boldsymbol{\tau}\}$, while the combined variables (a_{2i-1}, b_{2i-1}) can take the values $\{(\mathbf{1}, \mathbf{1}), (\mathbf{1}, \boldsymbol{\tau}), (\boldsymbol{\tau}, \mathbf{1}), (\boldsymbol{\tau}, \boldsymbol{\tau})\}$, but there are constraints on which values of (a_{2i-1}, b_{2i-1}) and d_{2i} can occur next to each other. From the fusion rules, it easily follows that the combinations of variables that are consistent with one another, have to be adjacent on the 'height graph', as shown in figure 13.

Hereafter, we will refer to the allowed variables (or pairs of variables on the odd sublattice) as 'heights'. The Hilbert space of the ladder model consists of all height configurations on a chain of length L, in such a way that two heights on neighboring sites also have to be neighbors (i.e. be connected by a solid line) in the height diagram of figure 13. In this way, the model can be mapped on the D_6 version of the RSOS model and, precisely when $J_r = J_p = \pm 1$, the model is critical, and can be solved exactly. We will not go into the details here (which can be found in [28]), but we will quickly state the result for this critical behavior in the original,

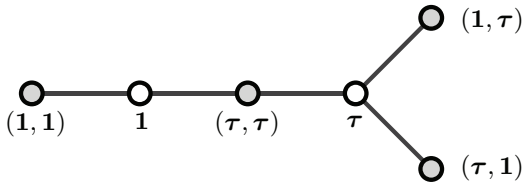

Figure 13. The allowed 'height' configurations of the ladder models. This diagram is the Dynkin diagram of the Lie algebra $D_6 = \mathrm{so}(12)$.

Fibonacci anyon setting, followed by the results for the Galois-conjugated Yang–Lee ladder. The details of the phase diagram, which closely mimics the phase diagram of the unitary ('not Galois-conjugated') ladder, and the numerical results will be presented in the next subsection.

As was the case for the chain models, also in the ladder case do the parts of the Hamiltonian form a representation of the Temperley–Lieb algebra, but in this case, the algebra is that [41] based on the Dynkin diagram D_6. The possible associated values of the d-isotopy parameter are given by $d = 2\cos(\frac{m_j\pi}{h})$, where $h = 10$, and the m_j are the exponents of the Lie algebra D_6, namely $m_j = 1, 3, 5, 7, 9, 5$. In the original ladder model $m_j = 1$, for both cases $J_r = J_p = \pm 1$. The associated value of the d-isotopy reads $d = 2\cos(\pi/10) = \sqrt{2+\phi}$. In the antiferromagnetic case, i.e. $J_r = J_p = 1$, or in the parameterization $J_p = \cos\theta$, $J_r = \sin\theta$, the point $\theta = \pi/4$, the critical behavior is described by the minimal model $\tilde{\mathcal{M}}(9, 10)$, which has central charge $c = 14/15$. With the tilde, we denote that we are considering the (A_8, D_6) modular invariant [52, 53], instead of the 'usual' (diagonal) (A_8, A_9) invariant[10].

We will now turn our attention to the Galois-conjugated version of the ladder model. The phase diagram of the Yang–Lee ladder is depicted in figure 11, and the location of the gapped phases, as well as the critical behavior, is exactly the same as in the Fibonacci ladder model. Therefore, we will be somewhat brief in the description of these phases (see the introduction of this section for a brief description of the gapped phases), and focus on the differences, which occur at the exactly solvable points, namely $\theta = \pi/4, 5\pi/4$, where the model is critical, but with a different critical behavior in comparison to the Fibonacci ladder.

The antiferromagnetic ($\theta = \pi/4$) *critical point.* As was the case in the Yang–Lee chains, the critical behavior of the Galois-conjugated model is obtained by picking a different d-isotopy parameter, corresponding to the Galois conjugate under consideration. For Fibonacci anyons, there is only one Galois conjugate, but nevertheless there seem to be different possible values for the d-isotopy parameter, namely $d = 2\cos(\frac{m_j\pi}{h})$, with $h = 10$, and $m_j = 1, 3, 5, 7, 9, 5$. In fact, the value we need is $m_j = 3$, which corresponds to the value obtained from the Fibonacci case, under Galois conjugation, namely $d = \sqrt{2 - 1/\phi} = 2\cos(3\pi/10)$.

It is a simple matter to check that this value corresponds to a model with central charge $c = 8/35$, by using the same arguments as those we presented in section 2.6. This central charge corresponds to the central charge of the non-unitary minimal model $\mathcal{M}(7, 10)$. Just as in the unitary case [28], the critical CFT describing the Yang–Lee model at $\theta = \pi/4$ is not the usual ('diagonal') modular invariant, but rather the (A, D) invariant or, to be more precise, (A_6, D_6). See [53] for information on the different modular invariants of the minimal models. We will denote this model by $\widetilde{\mathcal{M}}(7, 10)$. The field content of these models is given in tables 5 and 6 below. The details of the spectrum of this model will be discussed in section 3.4.

[10] We note that the (A_8, D_6) invariant minimal model $\widetilde{\mathcal{M}}(9, 10)$ is equivalent to the coset model $(G_2)_1 \times (G_2)_1/(G_2)_2$, where $(G_2)_k$ denotes the Wess–Zumino–Witten CFT at level k based on the Lie algebra G_2.

Table 4. Gapless theories for the ladder models.

Coupling	CFT	Central charge	d-isotopy
Fibonacci ladder			
AFM ($\theta = \pi/4$)	$\mathcal{M}(9, 10)$	$c = 14/15$	$2\cos(\pi/10)$
FM ($\theta = 5\pi/4$)	$\mathcal{Z}_8$ parafermion	$c = 7/5$	$2\cos(\pi/10)$
Yang–Lee ladder			
AFM ($\theta = \pi/4$)	$\widetilde{\mathcal{M}}(7, 10)$	$c = 8/35$	$2\cos(3\pi/10)$
FM ($\theta = 5\pi/4$)	$\widetilde{\mathcal{M}}(3, 10)$	$c = -44/5$	$2\cos(7\pi/10)$

Table 5. Kac table for the non-unitary minimal models $\mathcal{M}(7, 10)$ and $\mathcal{M}(3, 10)$. Only odd values of s are displayed, so that each field appears only once.

	$\mathcal{M}(7, 10)$			$\mathcal{M}(3, 10)$
$h(r, s)$	$s = 1$	3	5	$s = 1$
$r = 1$	0	13/7	46/7	0
2	1/40	247/280	1287/280	−11/40
3	2/5	9/35	104/35	−2/5
4	9/8	−1/56	95/56	−3/8
5	11/5	2/35	27/35	−1/5
6	29/8	27/56	11/56	1/8
7	27/5	44/35	−1/35	3/5
8	301/40	667/280	27/280	49/40
9	10	27/7	4/7	2

The ferromagnetic ($\theta = 5\pi/4$) *critical point*. In the non-unitary case, we can obtain the critical theory for the opposite sign of the interaction, by simply swapping the sign of the d-isotopy parameter, which hence corresponds to the value $d = 2\cos(7\pi/10) = -\sqrt{2 - (1/\phi)}$, from which it is a simple matter to extract the central charge, which is given by $c = -44/5$, corresponding to the minimal model $\mathcal{M}(3, 10)$. This minimal model also comes in two incarnations, one corresponding to the modular invariant (A_2, A_9), and the other to (A_2, D_6). (The field content of these models is also given in tables 5 and 6.) The latter is realized in the Yang–Lee ladder at $\theta = 5\pi/4$, and we will describe the spectrum in more detail below. Before we do that, however, we will first summarize the critical theories of both the Fibonacci and the Yang–Lee anyon ladders in table 4.

3.4. Numerical results

We finally present the numerical spectra of the conjugated ladder model at the two critical points discussed in the previous section. The spectrum for the critical point at $\theta = \pi/4$ is given in figure 14, where we indicated the locations of the primary fields of $\widetilde{\mathcal{M}}(7, 10)$ (given in table 6) by green squares, as well as some low-lying descendants with red circles. As usual, there are only two free parameters to match the numerically obtained spectrum with the result obtained from CFT, so the fact that the six lowest primaries, as well as several descendants, match to high precision (limited by finite-size effects) is a very non-trivial check on our results.

Table 6. Kac table for the '(A, D)-modular invariant' non-unitary minimal models $\widetilde{\mathcal{M}}(7, 10)$ and $\widetilde{\mathcal{M}}(3, 10)$. The fields with the conformal dimensions in bold (i.e. those with label $r = 5$) appear twice.

	$\widetilde{\mathcal{M}}(7, 10)$			$\widetilde{\mathcal{M}}(3, 10)$
$h(r, s)$	$s = 1$	3	5	$s = 1$
$r = 1$	0	13/7	4/7	0
3	2/5	9/35	−1/35	−2/5
5	**11/5**	**2/35**	**27/35**	**−1/5**

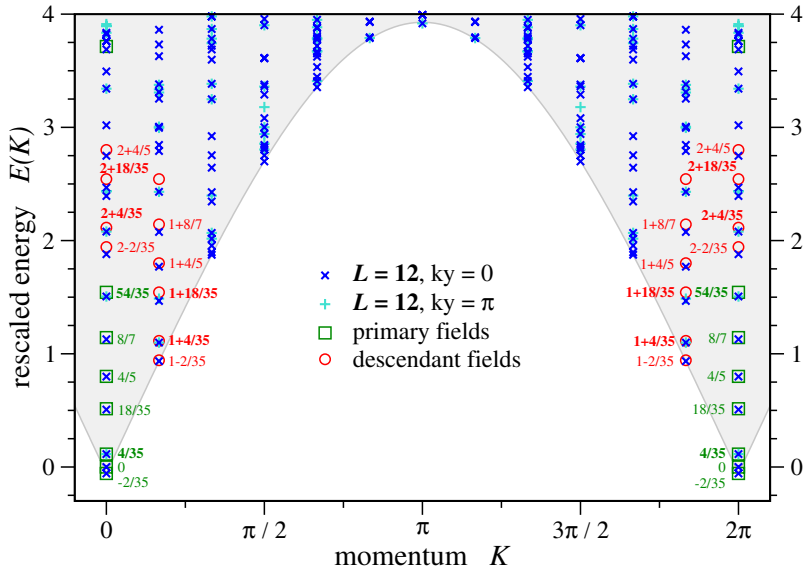

Figure 14. Conformal energy spectrum of the critical points in the doubled 'antiferromagnetic' Yang–Lee chain. The spectrum matches the non-unitary minimal model $\widetilde{M}(7, 10)$ with central charge $c = 8/35$. Primary fields of the CFT are indicated by green squares, descendant fields by red circles.

In figure 15, we give the numerical spectrum of the ferromagnetic Yang–Lee ladder, at $\theta = 5\pi/4$, which is characteristic of the critical phase extending over $\theta \in (\pi, 3\pi/2)$. In this case, the critical behavior is described by the $\widetilde{\mathcal{M}}(3, 10)$ non-unitary CFT and, as for the antiferromagnetic case, we were able to identify the primary fields, as well as several low-lying descendant fields, as indicated in the figure. The fields of the CFT are given in table 6.

4. Discussion and summary

In this paper, we studied the collective states of Yang–Lee anyons, a family of non-unitary, non-Abelian anyons that are close cousins of the unitary Fibonacci anyons. Non-unitary anyons of this form have attracted interest in the context of studies of certain quantum Hall wave functions, including the Gaffnian state [17]. Both Yang–Lee and Fibonacci anyons arise from the same anyonic theory, $su(2)_3$, and in particular they share the same fusion rules. The key distinction

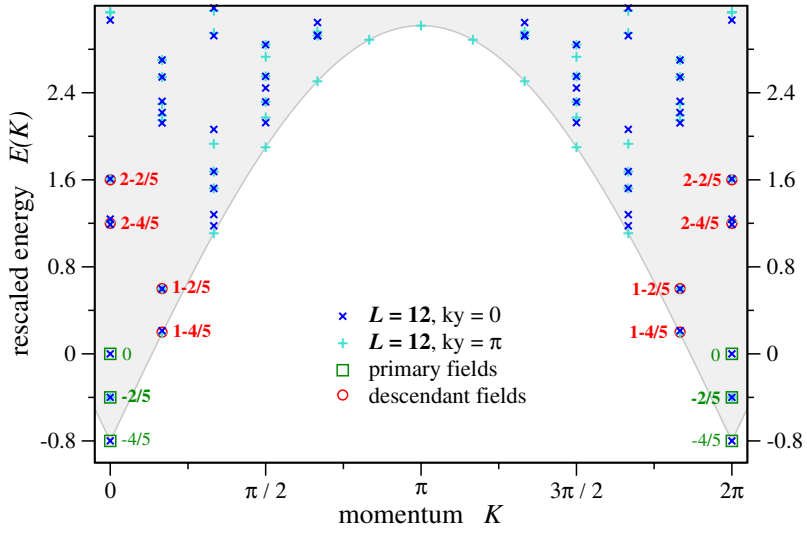

Figure 15. Conformal energy spectrum of the critical points in the doubled 'ferromagnetic' Yang–Lee chain. The spectrum matches the non-unitary minimal model $\widetilde{M}(3, 10)$ with central charge $c = -44/5$. Primary fields of the CFT are indicated by green squares and descendant fields by red circles.

between the two anyon types is that Yang–Lee anyons are non-unitary and relate to their unitary counterparts, the Fibonacci anyons, via 'Galois conjugation'. We have generalized this concept to arbitrary $su(2)_k$ anyonic theories.

To characterize the collective states formed by a set of anyons in the presence of pairwise interactions, we have considered 1D models of interacting Yang–Lee anyons similar to the golden chain model of the unitary case [23]. Analogous to the case of interacting Fibonacci anyons, the collective states of such chains of Yang–Lee anyons are found to be critical and the gapless theories are described by certain non-unitary CFTs (which depend on the sign of the coupling, see table 3).

The non-unitary chain models are found to exhibit rather peculiar features related to the presence of a non-local, topological symmetry first observed in the unitary models. For the multicritical gapless theories of these chain models this topological symmetry, whose related symmetry operator commutes with the Hamiltonian, allows us to classify all operators by a topology symmetry sector. It turns out that all relevant operators corresponding to (uniform) perturbations of the gapless system are in a different symmetry sector from the one of the ground state. In the unitary case, this mechanism that effectively protects the gapless ground state from local perturbations has led to an interpretation [34] of these gapless modes of a chain of interacting anyons as *edge states* of the parent topological liquid of which the anyons are excitations of. This has further led to the conclusion that interactions between anyons (in 2D arrangements) result in a splitting of the macroscopic degeneracy of a set of non-Abelian anyons and the nucleation of a new topological liquid inside and spatially separated from the parent liquid of which the anyons are excitations [34, 35].

For the non-unitary models, studied in this paper, a crucial distinction comes in the symmetry sector assigned to the ground state. While in the unitary case, the ground state was found to be in the flux-free (topological trivial) sector, we find that the ground state in the

non-unitary case exhibits a non-trivial topological flux (i.e. is in the non-trivial topological symmetry sector). It remains an open question whether such a spontaneous creation of topological flux can occur in the ground state of a system of interacting anyonic quasiparticles residing in a bulk-gapped topological liquid, which has no topological flux associated with it. This may be an indication that the non-unitary anyons are not massive quasiparticles of a gapped quantum liquid, but in fact excitations of a gapless quantum liquid.

In summary, we have investigated 1D models of non-unitary anyons based on $su(2)_k$ anyonic theories. The collective ground states are found to display critical behavior, similar to their unitary counterparts to which they are related via a 'Galois conjugation'. We described in detail the non-unitary CFTs, capturing their critical behavior, and commented on possible physical implications of our results in connection with proposed quantum Hall states related to such non-unitary CFTs. In addition, we also studied the phase diagram of an interacting ladder model, which is a quasi 1D version of the Levin–Wen model for non-unitary Yang–Lee anyons.

Acknowledgments

We are grateful for discussions with P Bonderson, M Freedman, J Slingerland and Z Wang. AWWL was supported in part by NSF DMR-0706140. We thank the Aspen Center for Physics and the Kavli Institute for Theoretical Physics, which is supported by NSF PHY-0551164. Our numerical work used some of the ALPS libraries [54, 55]; see also http://alps.comp-phys.org.

Appendix. A detailed description of the conformal energy spectra

In this section, we will describe in some detail the structure of the descendant fields present in the numerically obtained spectra. In the case of the Yang–Lee ladders, this structure is somewhat different from the 'usual' structure. The object containing information about the number of states at a specific energy and momentum (in the thermodynamic limit) is the partition function, which we will denote by Z_{tot}.

Modular invariance of the partition function on the torus constrains the possible partition functions of rational CFTs at a particular central charge [53]. In this paper, we will only be concerned with the partition functions of minimal models, which are described in terms of the chiral characters associated with the primary fields. An explicit expression for these chiral characters associated with the primary fields $\phi_{(r,s)}$ of the minimal models $\mathcal{M}(p, p')$ is given in, for instance, chapter 8 of [56].

$$\mathrm{ch}^{(p,p')}_{(r,s)}(q) = \frac{q^{h_{(r,s)}}}{(q)_\infty} \sum_{k\in\mathbb{Z}} \left(q^{k(kpp'+rp-sp')} - q^{(kp+s)(kp'+r)} \right), \tag{A.1}$$

where $(q)_\infty = \prod_{k>0}(1-q^k)$, and $h_{(r,s)} = \frac{(pr-p's)^2-(p-p')^2}{4pp'}$ the conformal dimension of the field $\phi_{(r,s)}$.

Dropping the labels (p, p'), all the possible partition functions can be written as

$$Z_{\mathrm{tot}} = \sum_{(r,s);(r',s')} M_{(r,s);(r',s')} \mathrm{ch}_{(r,s)} \mathrm{ch}^*_{(r',s')}. \tag{A.2}$$

For the minimal models, there is always the so-called 'diagonal modular invariant', for which M is diagonal, $M_{(r,s);(r',s')} = \delta_{r,r'}\delta_{s,s'}$, and the sum in the partition function runs over all primary

fields. However, in general, there exist other modular invariant partition functions. The critical points of the ladder models realize some of these, as we pointed out in the main text.

In terms of the Virasoro generators L_0 and $\bar{L}_0$, the Hamiltonian and momentum operators can be written (after an appropriate rescaling and shift) as $H = L_0 + \bar{L}_0$ and $P = (L_0 - \bar{L}_0)$. The partition function can be written as a trace over the Hilbert space, $Z_{\text{tot}} = \text{tr}\, q^{L_0}\bar{q}^{\bar{L}_0}$, which allows us to extract both the energies and momenta for each state.

In particular, the energy of a state is given by the sum of the powers of q and $\bar{q}$. We note that this energy is measured with respect to the energy corresponding to the energy of the identity operator $\mathbf{1}$, which we have set to zero. In addition, the momentum of a state is given by $L_0 - \bar{L}_0$, in units of $2\pi/L$, and measured with respect to the momentum of the corresponding primary field, which is not determined by CFT, but rather by the specific Hamiltonian realization.

A.1. The ferromagnetic Yang–Lee ladder

The critical theory describing the ferromagnetic Yang–Lee ladder is the (D_6, A_2) modular invariant $\widetilde{\mathcal{M}}(3, 10)$. The total partition function of this theory can be written as follows [53] (we will drop the labels $(p, p') = (3, 10)$ from the characters for convenience):

$$Z = |\text{ch}_{(1,1)}|^2 + |\text{ch}_{(3,1)}|^2 + 2|\text{ch}_{(5,1)}|^2 + |\text{ch}_{(7,1)}|^2 + |\text{ch}_{(9,1)}|^2 + (\text{ch}_{(1,1)}\text{ch}^*_{(1,2)} + \text{ch}_{(3,1)}\text{ch}^*_{(3,2)} + \text{c.c.}). \tag{A.3}$$

By expanding the partition function, in terms of q and $\bar{q}$, we can completely explain the low-lying part of the spectrum displayed in figure 15. Let us start with the vacuum sector of the theory, which corresponds to the part of the partition function with integer powers of q and $\bar{q}$:

$$Z_0 = |\text{ch}_{(1,1)}|^2 + |\text{ch}_{(9,1)}|^2 + (\text{ch}_{(1,1)}\text{ch}^*_{(1,2)} + \text{c.c.}) = 1 + 2q^2 + 2\bar{q}^2 + \cdots. \tag{A.4}$$

The total power of q and $\bar{q}$ gives the energy of the states, while the difference between the powers gives the momentum. Thus, the character of the vacuum sector implies the presence of two states at energy $E = 2$ and $K_x = 2$ as well as two states at energy $E = 2$ and momentum $K_x = -2$. Note that we count the states irrespective of their K_y sector.

We will continue with the descendants corresponding to the primary field with energy $E = -2/5$ and momentum $K_x = 0$. At this energy and momentum, there are in fact two states. This sector of the partition function reads

$$Z_{-2/5} = 2|\text{ch}_{(5,1)}|^2 = 2q^{-1/5}\bar{q}^{-1/5}(1 + q + \bar{q} + 2q^2 + 2\bar{q}^2 + q\bar{q} + \cdots), \tag{A.5}$$

which implies two states at $(E, K_x) = (1 - 2/5, 1)$ and two at $(E, K_x) = (1 - 2/5, -1)$, as well as two states at $(2 - 2/5, 0)$ and four at both $(2 - 2/5, 2)$ and $(2 - 2/5, -2)$, all of which is reproduced (modulo finite size effects) in the spectrum in figure 15.

Finally, we consider the descendants corresponding to the primary field at $E = -4/5$, which also has momentum $K_x = 0$. This sector of the partition function reads

$$\begin{aligned} Z_{-4/5} &= |\text{ch}_{(3,1)}|^2 + |\text{ch}_{(7,1)}|^2 + (\text{ch}_{(3,1)}\text{ch}^*_{(3,2)} + \text{c.c.}) \\ &= q^{-2/5}\bar{q}^{-2/5}\left(1 + 2q + 2\bar{q} + 3q^2 + 3\bar{q}^3 + 4q\bar{q} + \cdots\right). \end{aligned} \tag{A.6}$$

This implies the presence of two states at both $(E, K_x) = (1 - 4/5, 1)$ and $(1 - 4/5, 1)$, as well as three states at both $(2 - 4/5, 2)$ and $(2 - 4/5, -2)$. In addition, there should be four states at $(2 - 4/5, 0)$. This seems to be at odds with figure 15, but it turns out that the state at $K_x = 0$ and $K_y = \pi$, and energy of approximately $E \approx 2 - 4/5$ (or, more precisely, $E \approx 1.214\,4495$) is in fact doubly degenerate, so indeed, there are four states, as expected from the partition function.

A.2. The antiferromagnetic Yang–Lee ladder

A similar analysis can be performed for the antiferromagnetic critical point of the Yang–Lee ladder. We will be brief here, because the analysis is identical to the one for the ferromagnetic critical point.

There are nine sectors in this particular case, corresponding to the fields displayed in table 6, so the partition function can be written as

$$Z_{\mathrm{tot}} = Z_0 + Z_{4/5} + Z_{22/5} + Z_{26/7} + Z_{18/35} + Z_{4/35} + Z_{8/7} + Z_{-2/35} + Z_{54/35}. \qquad \text{(A.7)}$$

Although we will not consider all of these sectors (some give rise to states that are too high in energy to be unambiguously identified, due to finite size effects), we will nevertheless give the form of the partition function restricted to each of these sectors. We will drop the labels $(p, p') = (7, 10)$ from the characters

$$\begin{aligned}
Z_0 &= |\mathrm{ch}_{(1,1)}|^2 + |\mathrm{ch}_{(9,1)}|^2 + (\mathrm{ch}_{(1,1)}\mathrm{ch}^*_{(1,6)} + \text{c.c.}),\\
Z_{4/5} &= |\mathrm{ch}_{(3,1)}|^2 + |\mathrm{ch}_{(7,1)}|^2 + (\mathrm{ch}_{(3,1)}\mathrm{ch}^*_{(3,6)} + \text{c.c.}),\\
Z_{22/5} &= 2|\mathrm{ch}_{(5,1)}|^2,\\
Z_{26/7} &= |\mathrm{ch}_{(1,3)}|^2 + |\mathrm{ch}_{(9,3)}|^2 + (\mathrm{ch}_{(1,3)}\mathrm{ch}^*_{(1,4)} + \text{c.c.}),\\
Z_{18/35} &= |\mathrm{ch}_{(3,3)}|^2 + |\mathrm{ch}_{(7,3)}|^2 + (\mathrm{ch}_{(3,3)}\mathrm{ch}^*_{(3,4)} + \text{c.c.}),\\
Z_{4/35} &= 2|\mathrm{ch}_{(5,3)}|^2,\\
Z_{8/7} &= |\mathrm{ch}_{(1,5)}|^2 + |\mathrm{ch}_{(9,5)}|^2 + (\mathrm{ch}_{(1,5)}\mathrm{ch}^*_{(1,2)} + \text{c.c.}),\\
Z_{-2/35} &= |\mathrm{ch}_{(3,5)}|^2 + |\mathrm{ch}_{(7,5)}|^2 + (\mathrm{ch}_{(3,5)}\mathrm{ch}^*_{(3,2)} + \text{c.c.}),\\
Z_{54/35} &= 2|\mathrm{ch}_{(5,5)}|^2.
\end{aligned}$$

The parts of the partition function read explicitly

$$\begin{aligned}
Z_0 &= 1 + q^2 + \bar{q}^2 + \cdots,\\
Z_{4/5} &= q^{2/5}\bar{q}^{2/5}\left(1 + q + \bar{q} + 2q^2 + q\bar{q} + 2\bar{q}^2 + \cdots\right),\\
Z_{22/5} &= 2q^{11/5}\bar{q}^{11/5}\left(1 + q + \bar{q} + 2q^2 + q\bar{q} + 2\bar{q}^2 + \cdots\right),\\
Z_{26/7} &= q^{13/7}\bar{q}^{13/7}\left(1 + q + \bar{q} + 3q^2 + q\bar{q} + 3\bar{q}^2 + \cdots\right),\\
Z_{18/35} &= q^{9/35}\bar{q}^{9/35}\left(1 + 2q + 2\bar{q} + 3q^2 + 4q\bar{q} + 3\bar{q}^2 + \cdots\right),\\
Z_{4/35} &= 2q^{2/35}\bar{q}^{2/35}\left(1 + q + \bar{q} + 2q^2 + q\bar{q} + 2\bar{q}^2 + \cdots\right),\\
Z_{8/7} &= q^{4/7}\bar{q}^{4/7}\left(1 + q + \bar{q} + q^2 + q\bar{q} + \bar{q}^2 + \cdots\right),\\
Z_{-2/35} &= q^{-1/35}\bar{q}^{-1/35}\left(1 + q + \bar{q} + 2q^2 + q\bar{q} + 2\bar{q}^2 + \cdots\right),\\
Z_{54/35} &= 2q^{27/35}\bar{q}^{27/35}\left(1 + q + \bar{q} + 2q^2 + q\bar{q} + 2\bar{q}^2 + \cdots\right).
\end{aligned}$$

With this information, it is rather straightforward to check that the primaries and descendant fields we indicated in figure 14 indeed come with the right multiplicities.

A.3. The ferromagnetic Yang–Lee chain

After having dealt with the (anti)ferromagnetic Yang–Lee ladders in quite some detail, we will content ourselves here by giving the (diagonal) partition functions describing the spectra, and note that for all states where finite size effects allow us to make an identification, we obtain full agreement with the CFT prediction.

The partition function in the case of the ferromagnetic Yang–Lee chain, the critical model is given by the diagonal invariant of the model $\mathcal{M}(2, 5)$, whose partition function reads (dropping the label (2, 5) on the chiral character)

$$Z = |\mathrm{ch}_{(1,1)}|^2 + |\mathrm{ch}_{(3,1)}|^2 = Z_0 + Z_{-2/5}, \tag{A.8}$$

with

$$\begin{aligned} Z_0 = 1 &+ q^2 + \bar{q}^2 + q^3 + \bar{q}^3 + q^4 + q^2\bar{q}^2 + \bar{q}^4 + q^5 + q^3\bar{q}^2 + q^2\bar{q}^3 + \bar{q}^5 \\ &+ 2q^6 + q^4\bar{q}^2 + q^3\bar{q}^3 + q^2\bar{q}^4 + 2\bar{q}^6 + \cdots, \end{aligned} \tag{A.9}$$

$$\begin{aligned} Z_{-2/5} = q^{-1/5}\bar{q}^{-1/5}(&1 + q + \bar{q} + q^2 + q\bar{q} + \bar{q}^2 + q^3 + q^2\bar{q} + q\bar{q}^2 + \bar{q}^3 + 2q^4 + q^3\bar{q} + q^2\bar{q}^2 + q\bar{q}^2 + 2\bar{q}^4 \\ &+ 2q^5 + 2q^4\bar{q} + q^2\bar{q}^3 + q^3\bar{q}^2 + 2q\bar{q}^4 + 2\bar{q}^5 + 3q^6 + 2q^5\bar{q} + 2q^4\bar{q}^2 \\ &+ q^3\bar{q}^3 + 2q^2\bar{q}^4 + 2q\bar{q}^5 + 3\bar{q}^6 + \cdots). \end{aligned} \tag{A.10}$$

All these states, and in fact quite a few more that we did not give here, are reproduced in the spectrum of the ferromagnetic Yang–Lee chain, as shown in figure 8.

A.4. The antiferromagnetic Yang–Lee chain

Finally, we deal with the antiferromagnetic Yang–Lee chain, the critical behavior of which is described by the (diagonal invariant of the) minimal model $\mathcal{M}(3, 5)$, which has four primary fields, as described in the main text. The relevant partition function is given by (again, dropping the labels (3, 5) on the chiral characters)

$$Z = |\mathrm{ch}_{(1,1)}|^2 + |\mathrm{ch}_{(3,1)}|^2 + |\mathrm{ch}_{(1,2)}|^2 + |\mathrm{ch}_{(3,2)}|^2 = Z_0 + Z_{2/5} + Z_{3/2} + Z_{-1/10}, \tag{A.11}$$

with

$$\begin{aligned} Z_0 &= 1 + q^2 + \bar{q}^2 + \cdots, \\ Z_{2/5} &= q^{1/5}\bar{q}^{1/5}(1 + q + \bar{q} + 2q^2 + q\bar{q} + 2\bar{q}^2 + \cdots), \\ Z_{3/2} &= q^{-3/4}\bar{q}^{-3/4}(1 + q + \bar{q} + \cdots), \\ Z_{-1/10} &= q^{1/20}\bar{q}^{1/20}(1 + q + \bar{q} + q^2 + q\bar{q} + \bar{q}^2 + 2q^3 + q^2\bar{q} + q\bar{q}^2 + 2\bar{q}^3 \cdots). \end{aligned} \tag{A.12}$$

We should note that, as can be seen in figure 7, these fields are reproduced, and that (for $L = 32$ sites), the fields with conformal dimension $h = -1/20$ and $h = 3/4$ occur at momentum $K_x = 0$, while the identity fields and the field with conformal dimension $h = 1/5$ occur at momentum $K_x = \pi$.

References

[1] Leinaas J M and Myrheim J 1977 *Nuovo Cimento* B **77** 1
[2] Wilczek F 1982 *Phys. Rev. Lett.* **49** 957
[3] Moore G and Read N 1991 *Nucl. Phys.* B **360** 362
[4] Read N and Green D 2000 *Phys. Rev.* B **61** 10267
[5] Cooper N R, Wilkin N K and Gunn J M F 2001 *Phys. Rev. Lett.* **87** 120405
[6] Fu L and Kane C L 2008 *Phys. Rev. Lett.* **100** 096407
[7] Willet R L, Pfeiffer L N and West K W 2009 *Proc. Natl Acad. Sci. USA* **106** 8853
[8] Bid A, Ofek N, Inoue H, Heiblum M, Kane C, Umansky V and Mahalu D 2010 *Nature* **466** 585
[9] Haldane F D M and Rezayi E H 1988 *Phys. Rev. Lett.* **60** 956
[10] Wen X-G and Wu Y-S 1994 *Nucl. Phys.* B **419** 455
[11] Milovanovič M and Read N 1996 *Phys. Rev.* B **53** 13559
[12] Gurarie V 1993 *Nucl. Phys.* B **410** 535
[13] Gurarie V, Flohr M and Nayak C 1997 *Nucl. Phys.* B **498** 513
[14] Guruswamy S and Ludwig A W W 1998 *Nucl. Phys.* B **519** 661
[15] Read N 2009 *Phys. Rev.* B **79** 245304
[16] Read N 2009 *Phys. Rev.* B **79** 045308
[17] Simon S H, Rezayi E H, Cooper N R and Berdnikov I 2007 *Phys. Rev.* B **75** 075317
[18] Read N and Green D 2000 *Phys. Rev.* B **61** 10267
[19] Simon S H, Rezayi E H and Cooper N R 2007 *Phys. Rev.* B **75** 075318
[20] Bernevig B A and Haldane F D M 2008 *Phys. Rev. Lett.* **101** 246806
[21] Estienne B and Santachiara R 2009 *J. Phys. A: Math. Theor.* **42** 445209
[22] Simon S H, Rezayi E H and Regnault N 2010 *Phys. Rev.* B **81** 121301
[23] Feiguin A, Trebst S, Ludwig A W W, Troyer M, Kitaev A, Wang Z and Freedman M H 2007 *Phys. Rev. Lett.* **98** 160409
[24] Forrester P J and Baxter R J 1984 *J. Stat. Phys.* **35** 193
[25] Andrews G E, Baxter R J and Forrester P J 1984 *J. Stat. Phys.* **35** 193
[26] de Boer J and Goeree J 1991 *Commun. Math. Phys.* **139** 267
[27] Coste A and Gannon T 1994 *Phys. Lett.* B **323** 316
[28] Gils C, Trebst S, Kitaev A, Ludwig A W W, Troyer M and Wang Z 2009 *Nat. Phys.* **5** 834
[29] Bonesteel N E and Yang K 2007 *Phys. Rev. Lett.* **99** 140405
[30] Trebst S, Ardonne E, Feiguin A, Huse D A, Ludwig A W W and Troyer M 2008 *Phys. Rev. Lett.* **101** 050401
[31] Trebst S, Troyer M, Wang Z and Ludwig A W W 2008 *Prog. Theor. Phys. Suppl.* **176** 384
[32] Fidkowski L, Refael G, Bonesteel N E and Moore J E 2008 *Phys. Rev.* B **78** 224204
[33] Fidkowski L, Lin H-H, Titum P and Refael G 2009 *Phys. Rev.* B **79** 155120
[34] Gils C, Ardonne E, Trebst S, Ludwig A W W, Troyer M and Wang Z 2009 *Phys. Rev. Lett.* **103** 070401
[35] Ludwig A W W, Poilblanc D, Trebst S and Troyer M 2011 *New J. Phys.* **13** 045014
[36] Kassel C 1995 *Quantum Groups* (New York: Springer)
[37] Bonderson P 2009 *Phys. Rev. Lett.* **103** 110403
[38] Ardonne E and Slingerland J K 2010 *J. Phys. A: Math. Theor.* **43** 395205
[39] Etingof P, Nikshych D and Ostrik V 2005 *Ann. Math.* **162** 581
[40] Kirillov A N and Reshetikhin N Y 1988 Representations of the algebra $U_q(sl(2))$, q-orthogonal polynomials and invariants of links *Proc. Conf. on Infinite Dimensional Lie Algebras and Groups* (*CIRM, Luminy, Marseille, 1988*) ed V G Kac (Singapore: World Scientific) p 285
[41] Pasquier V 1987 *Nucl. Phys.* B **285** 162
[42] Temperley N and Lieb E 1971 *Proc. R. Soc. Lond.* A **322** 251
[43] Baxter R J 1982 *Exactly Solved Models in Statistical Mechanics* (London: Academic)
[44] Huse D A 1984 *Phys. Rev.* B **30** 3908

[45] Riggs H 1989 *Nucl. Phys.* B **326** 673
[46] Nakanishi T 1990 *Nucl. Phys.* B **334** 745
[47] Yang C N and Lee T D 1952 *Phys. Rev.* **87** 404
Yang C N and Lee T D 1952 *Phys. Rev.* **87** 410
[48] Cardy J L 1985 *Phys. Rev. Lett.* **54** 1354
[49] Dotsenko Vl S and Fateev V A 1984 *Nucl. Phys.* B **240** 312
[50] Nienhuis B 1984 *J. Stat. Phys.* **34** 731
[51] Levin M A and Wen X G 2005 *Phys. Rev.* B **71** 045110
[52] Cardy J L 1986 *Nucl. Phys.* B **270** 186
[53] Cappelli A, Itzykson C and Zuber J-B 1987 *Nucl. Phys.* B **280** 445
[54] Bauer B *et al* 2011 *J. Stat. Mech.* at press (preprint arXiv:1101.2646)
[55] Albuquerque F *et al* 2007 *J. Magn. Magn. Mater.* **310** 1187
[56] Di Francesco P, Mathieu P and Sénéchal D 1999 *Conformal Field Theory* (New York: Springer)